Amorphous Si/SiC phototransistors and avalanche photodiodes

C.Y. Chang
J.W. Hong
Y.K. Fang

Indexing terms: Semiconductor devices and materials, Diodes, Transistors

Abstract: The device structures, operation principles, optoelectronic characteristics, performance comparisons, and possible applications for various a-Si:H/a-SiC:H phototransistors and avalanche photodiodes are reviewed. Although these devices are made of amorphous semiconductors, its majority-carrier transport properties can tactfully avoid gap-state and defect related minority-carrier transport problems, and obtain good performances. Also, each of these devices has the distinct advantage of meeting the requirements of different practical applications. The unique and distinct advantages of these a-Si:H/a-SiC:H devices are first, a variety of peak response wavelengths are achievable by changing the composition or the well-to-barrier widths of the superlattice, secondly, a large-area-detector image sensor can be made on a glass substrate; and thirdly, the low-temperature of the amorphous films ($\sim$250°C) possesses a very abrupt composition change and a doping profile, which are impossible in the single-crystalline semiconductors.

1 Introduction

Recently, there has been a remarkable advance in both the physics and technologies of amorphous semiconductors. Their significant properties, such as the excellent photoconductivity and the mass-producability of large-area nonepitaxial growth on any substrate material, have attracted much attention as a new optoelectronic material. Tremendous research and development efforts have been made in areas including thin-film growth mechanism, improvement of the deposition process, device design and fabrication etc.. These new areas have opened up some new application fields such as the low-cost solar cell and the thin-film transistor (TFT). In the last few years, the applications of amorphous devices have extended to the light-emitting diode (LED), electro-photoreceptor, photoscanner, charge-coupled device (CCD) etc. [1–2]. The photosensing devices to be described in this paper are different from the conventional amorphous *p-i-n* photodiode or photoconductor. These amorphous devices not only have optical gain, but also possess other good optoelectronic characteristics.

The a-Si:H and a-SiC:H films in the devices to be described were deposited by using the Anelva model PED301 radio-frequency capacitance-coupled parallel-plate plasma enhanced chemical vapour deposition (PECVD) system. This system can deposit various films at a low temperature of about 250°C. Also, by varying the combination of input gases, this system can deposit multilayer thin-film continuously. With this kind of deposition system, it is easier to obtain the abrupt interface of materials and step junction of dopings for amorphous semiconductors, and hence, the amorphous semiconductor superlattice (SL). During the fabrication process, the substrate temperature was kept at 250°C and the chamber pressure was 1 torr. The RF power was 40 W for the undoped a-Si:H film, whereas it was 50 W for the heavily doped a-Si:H film and 30 W for the undoped and doped a-SiC:H films, respectively. The silane gas (75% H_2 + 25% SiH_4) was employed to deposit the a-Si:H films. The a-SiC:H layers were grown by the plasma decompositon of a gas mixture (45% SiH_4 + 55% CH_4). For doped a-Si:H and a-SiC:H films, the diluted phosphine (1% PH_3 + 99% H_2) and diborane (1% B_2H_6 and 99% H_2) were used as the dopants for *n*-type and *p*-type layers, respectively. The deposition rates of a-Si:H and a-SiC:H films were 1.67 and 0.67 Å/S individually. The band-gaps for the intrinsic a-Si:H and a-SiC:H are approximately 1.8 and 2.25 eV, respectively. When these two materials form a step heterojunction, the conduction and valence band discontinuities (ΔE_c and ΔE_V) are 0.35 and 0.1 eV, respectively.

All of the amorphous photosensing devices to be described in this paper were fabricated on the ITO (indium-tin oxide) coated glass substrate. The incident light penetrates the transparent glass and ITO electrode and is absorbed in the device interior. The other electrode of the devices is thermally evaporated Al film with a thickness of 5000 Å. The device area is 1.41×10^{-2} cm^2, except when noted otherwise. All of the devices are without antireflection coating on the glass surface.

2 Device structure, operation and characteristics of PT

Fig. 1 shows the schematic cross-section of an a-Si:H phototransistor (PT) [3–5]. As compared to the device structure of the conventional crystalline silicon (c-Si) *npn* bipolar junction transistor, the most evident difference is that there are two intrinsic a-Si:H layers of thickness d_1

Paper 7981J (E3, E13), first received 7th September 1990 and in revised form 24th January 1991

Chun-Yen Chang is with the Institute of Electronics, National Chiao Tung University, Hsinchu, Taiwan, Republic of China

Jyh-Wong Hong is with the Department of Electrical Engineering, National Central University, Chungli, Taiwan, Republic of China

Yean-Kuan Fang is with the Semiconductor and System Laboratories, National Cheng Kung University, Tainan, Taiwan, Republic of China

and d_2 which are interpolated into the amorphous base-emitter and base-collector *pn* junctions, respectively. These two *i*-layers are used to promote the operation

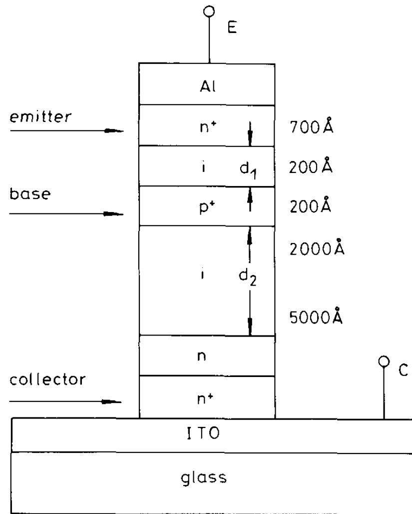

Fig. 1 *Schematic cross-section of a-Si:H PT*

voltage of the device and to reduce its leakage current. $d_2 = 3000$ Å, and is chosen by compromising the obtainable optical gain and the amount of light absorption. d_1 is chosen to be shorter than the Debye length of the base region, so, the entire base and both its sides, i.e. the *i*-layers, are completely depleted of free carriers at any bias condition. The ratio of d_1 and d_2 approximately determines the ratio of voltages across the two amorphous *p-i-n* junctions when the external bias $V_{CE} > 0$ is applied. The n^+-layer at the collector forms an ohmic contact to the ITO electrode [6–7].

Figs. 2*a* and *b* illustrate the schematic energy-band diagram of PT under equilibrium and normal operation

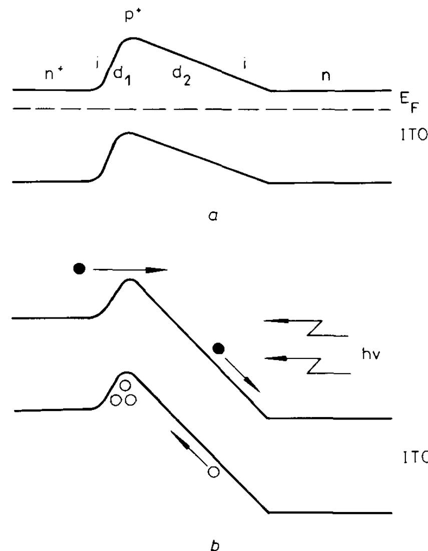

Fig. 2 *Schematic energy-band diagrams of a-Si:H PT*
a Under equilibrium condition
b Under normal bias ($V_{CE} > 0$) and illumination

($V_{CE} > 0$), respectively [2, 6, 7]. As can be seen in the Figures, a triangular potential is formed between the n^+-emitter and n^+-collector electrodes owing to the thin p^+ base region being depleted of free carriers. The total current of the device under dark or illumination for $V_{CE} > 0$ consists of an electron current, a hole current, and an additional generation-recombination (*g-r*) current. The dark electron current is due to the electrons traversing the triangular barrier by thermionic emission and then drifting down the barrier toward the collector. The dark hole current is essentially a diffusion current in the quasi-neutral emitter region. The dark *g-r* current includes a recombination current in the emitter *i*-layer, a generation current in the collector *i*-layer, and a recombination current in the thin base region. When light is incident on the glass substrate side and penetrates into the collector *i*-layer, the electron-hole pairs are generated. The photogenerated electrons drift down to the collector. The photogenerated holes drift down to its base valley and are partially accumulated in this valley. The accumulated holes (minority carriers) will neutralise the static negative charges in the base region and reduce the triangular potential barrier height. This induced barrier-lowering increases the electron (majority carrier) and hole current exponentially. The amount of this barrier-lowering can be estimated by using the principle of detailed balance, i.e. the photogenerated hole flux ($A\phi_L$, where A is the device area), recombines at a rate of the collector hole recombination current (I_{rc}) and is balanced by the hole current injected into the emitter (I_{p1}) and the hole recombination current in the base (I_{rb}) and emitter (I_{re}) regions. These hole recombination currents in the emitter, base and collector regions can be estimated by the *g-r* mechanism in each region individually. In the normal case, I_{re} and I_{rc} are negligible, since they are the excess hole recombination currents in emitter and collector regions, respectively. So, $A\phi_L \approx I_{pl} + I_{rb}$, and the amount of barrier-lowering ($\Delta\phi_L$) can be approximately expressed as [8]

$$\Delta\phi_L = (kT/q) \ln \frac{A\phi_L}{I_{ps} e^{qV_1/nkT} + A\bar{P}(e^{qV_1/nkT})/\tau_{eff}}$$

where $V_1 \approx d_1 V_{CE}/(d_1 + d_2)$, $\bar{P}$ is the total amount of excess holes per unit area in the base region under equilibrium. I_{ps} is the hole saturation current (for the dark hole current which diffuses across the quasi-neutral region of the emitter). τ_{eff} is the effective hole lifetime in the base, and is presumably due to band-to-band and capture-emission processes via traps. The electron and hole currents, and hence the total current and the photocurrent gain can be calculated after the amount of $\Delta\phi_L$ is estimated [8].

The main characteristics of the photosensing devices include photo I-V curves, optical gain, response time, and spectral response etc. In general the DC optical gain G can be expressed as [9]

$$G = [(I_p - I_d)/q]/(P_{in}/h\nu)$$

where I_p is the photocurrent under illumination, I_d the dark current, P_{in} the incident light power, $h\nu$ the energy of incident photon, and q the electron charge. For convenience, the He-Ne laser was used as the light source (wavelength $\lambda = 6328$ Å) during the measurements of optical gain and photo I-V curves. The optical gain is dependent of the bias voltage and incident light power level. An optimum bias is needed to obtain the highest optical gain. All of the photosensors described in this

paper are majority-carrier devices, so the optical gain increases with the decreasing P_{in}.

The response time (t_r) of the described photosensing devices was measured by illuminating the device with a light pulse emitted from a commercial LED (with a response time of 90 ns, a peak wavelength at 650 nm, and a full-width-half-maximum (FWHM) = 100 nm) excited by a square voltage wave, and monitoring the waveform of the collector current for the inverter-connected photosensor with a variable load resistor R_L. After obtaining the switching times, t_{on} and t_{off}, the response time $t_r = (t_{on} + t_{off})/2$ was calculated. t_r is interrelating to the junction capacitance and load resistance, and is also affected by the stray capacitance and the internal resistance of the device.

The relative spectral response of the devices was measured under a tungsten lamp through a monochrometer on the collector side. The incident wavelength ranges from 400 nm to 800 nm, covering all of the wavelengths of visible light.

For an a-Si:H PT, the peak optical gain is 12. The response time $t_r = 30\,\mu s$. The a-Si:H PT is the first amorphous device with gain and has a simple structure. There are two alternative device structures derived from this simple PT. One is to omit the emitter n^+ layer and use Al film to form a Schottky barrier emitter with the i-layer [6], the other is to omit the collector n-layer, retaining the n^+ layer to form an ohmic contact with ITO [6]. These two alternative devices have a similar operation principle and performance.

3 HPT

The schematic cross-section and the energy-band diagram under $V_{CE} = (V_1 + V_2) > 0$ for an a-Si:H/a-SiC:H heterojunction phototransistor (HPT) are depicted in Figs. 3*a* and *b*, respectively. In HPT, the emitter and base are made of the wide-gap a-SiC:H, which provides a more effective barrier to accumulate more photogenerated holes at the base. So, the $\Delta\phi_L$ increases, hence the electron current over the barrier, and the optical gain is improved [10–12].

The basic HPT has two alternative structures with similar performance. One is to replace the collector n^+ a-Si:H layer by a wide-gap n^+ a-SiC:H layer to increase the amount of light absorption by the optical window effect [11]. The other is to use the narrow-gap a-Si:H material in the thin base region to increase the amount of accumulated holes and then $\Delta\phi_L$. However, in this case, the conduction band has an electronic potential spike which disturbs the electron current, so, a suitable thickness of the thin a-Si:H base region should be chosen to increase the optical gain [13].

As compared to PT, the HPT has a higher optical gain (40), a shorter response time (10 μs), and particularly an interesting spectral response. Figs. 4*a* and *b* show the normalised spectral responses ranging from 400 to 800 nm, varying with different collector i-layer thickness d_2 and with different V_{CE} bias, respectively. As can be seen in Fig. 4*a*, when the d_2 thickness increases from 2000 Å to 7000 Å, the peak response shifts from 5500 Å to 6500 Å, and the FWHM also becomes narrower. This is because of the longer absorbing path in the d_2 region which especially favours the long-wavelength light. When the bias voltage V_{CE} increases from 1 to 7 and 13 V, the peak response shifts from 620 to 540 and 440 nm, respectively, as can be found from Fig. 4*b*. Both the thickness-dependent and voltage-dependent characteristics can be related to the field strength. As shown in Fig. 4*b*, the relative response at the shorter wavelengths increases with the increasing field strength, whereas the relative

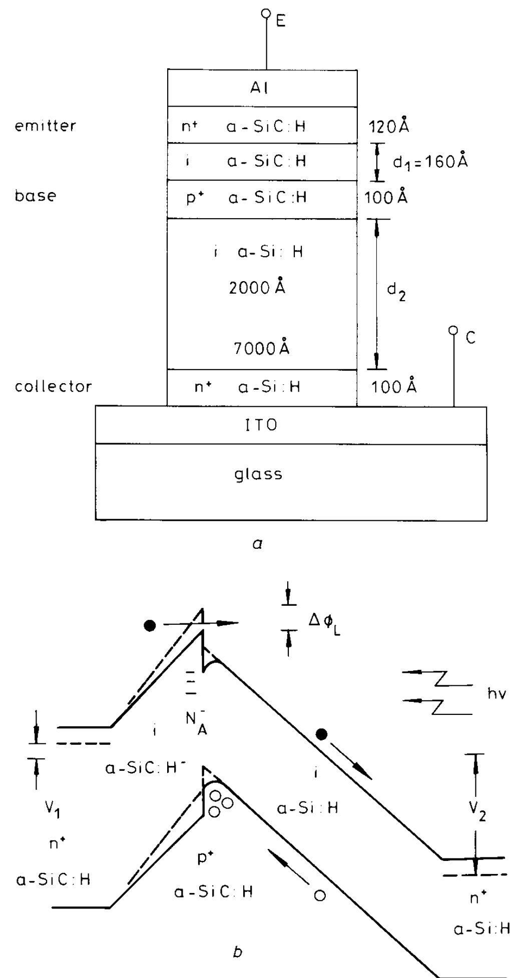

Fig. 3 *Cross-section view and energy-band diagram under normal operation for a-Si:H/a-SiC:H HPT*
a Cross-section view *b* Energy-band diagram

response at the longer wavelengths changes only slightly, which can be explained by the improvement of recombination loss and carrier collection efficiency under a higher electric field. Both of the voltage-dependent and thickness-dependent photo I-V characteristics provide the flexibility for designing a voltage-controllable colour-sensitive photodetector [10, 12].

4 Application of SL in PT and HPT

To improve the performances of the PT and HPT further, the intrinsic a-Si:H/a-SiC:H superlattice (SL) structures have been applied to the amorphous HPT and PT in their undoped collector light absorption regions, and are named as an a-Si:H/a-SiC:H superlattice heterojunction phototransistor (SHPT) and an a-Si:H/a-SiC:H superlattice phototransistor (SLPT), respectively. The a-Si:H/a-SiC:H heterojunction has a $\Delta E_v < \Delta E_c$, hence the electron impact ionisation rate (α) is larger than the hole impact ionisation rate (β). Therefore, the SL struc-

ture in the collector region could promote the electron multiplication and improve the optoelectronic characteristics of the amorphous HPT or PT, especially at a higher V_{CE} bias near the breakdown voltage [18–20].

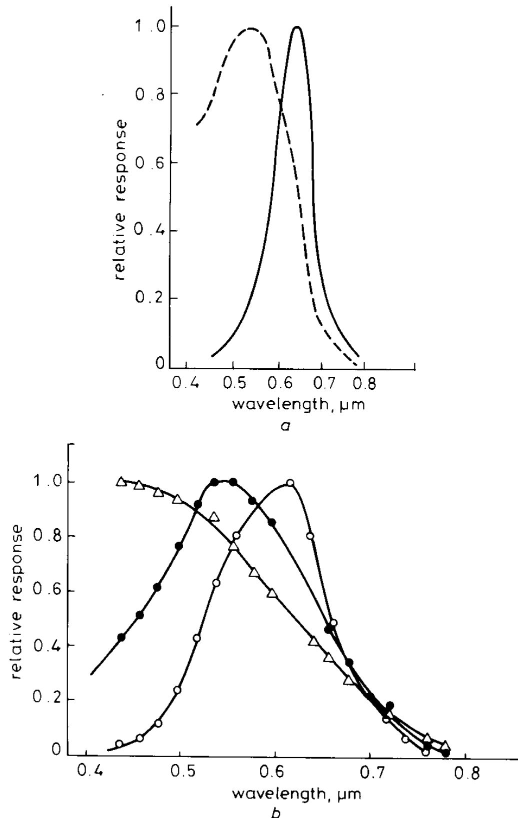

Fig. 4 *Normalised relative spectral responses of a-Si:H/a-SiC:H HPTs*

a With different collector thickness
b With different V_{CE} voltage applied for normal operation
$V_{CE} = 4$ V
—— $d_2 = 7000$ Å
- - $d_2 = 2000$ Å
○ $V_{CE} = 1$ V
● $V_{CE} = 7$ V
△ $V_{CE} = 13$ V
$d_2 = 3000$ Å

Figs. 5*a* and *b* illustrate the schematic cross-section and the simplified energy-band diagram, respectively, under normal operation ($V_{CE} > 0$) for SHPT. As shown in Fig. 5*a*, in addition to the SL structure, the collector region, near the base, has an intrinsic a-Si:H layer with thickness *S*. In the SL structure, the thickness of the a-Si:H well (t_w) is 80 Å and that of the a-SiC:H barrier (t_b) is 120 Å. The period number $N = 10$. It is found that the shapes of photo I-V curves for SHPT are much like those of a typical c-Si phototransistor. The optical gain can be as high as 78. The response time is only 4.1 µs. Hence, the SHPT operating in normal mode can be used as an optoelectronic linear amplifier and digital switching device. The thickness *S* can also be used to adjust the device breakdown voltage. When the thickness *S* increases from 500 to 3000 Å, the device breakdown voltage (at a dark current $I_d = 100$ µA) increases linearly from 22 to 40 V. When the thickness *S* is smaller, the amount of light absorption in SHPT is smaller. Otherwise, a larger thickness *S* results in a smaller electric field, which in turn weakens the impact ionisation in the SL and increases the device internal resistance. Based on a compromise between the optical gain and the obtainable breakdown voltage, an optimum $S = 2000$ Å. The relative spectral response of the SHPT has two peaks for a

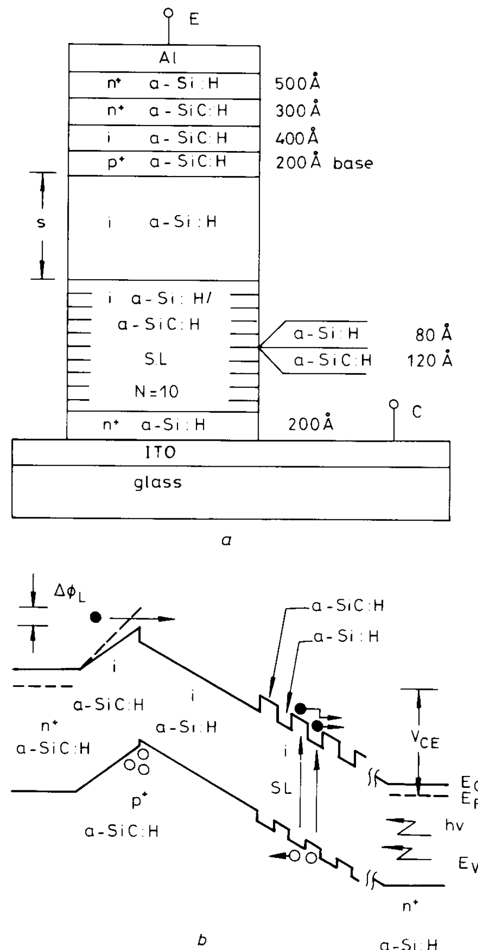

Fig. 5 *Device structure, and band diagram under normal operation for a-Si:H/a-siC:H SHPT*

a Device structure
b Band diagram

moderate V_{CE} voltage around 10 V. The main peak response at 560 nm is probably due to the effective band-gap of the a-Si:H/a-SiC:H SL ($E_g = 2.1$ eV). The sub-peak near 640 nm may be corresponding to the band-gap of the a-Si:H ($E_g = 1.8$ eV) layer with thickness *S* in the collector region. Increasing the V_{CE} voltage shifts the main peak toward a shorter wavelength and reduces the evidence of the sub-peak [17].

If the n^+ a-SiC:H (200 Å) base and the intrinsic a-Si:H layer with thickness *S* in SHPT are replaced by the $n(350$ Å$) - i(200$ Å$) - p(100$ Å$)$ a-Si:H layers, then the emitter junction becomes a homojunction and the SHPT changes to the above-mentioned SLPT. The SLPT has a higher internal electric field at similar V_{CE} bias levels, as compared to SHPT. So, the electron multiplication is stronger and the optical gain is higher [17].

In SLPT, the selected $t_b = 80$ Å and $t_w = 50 - 500$ Å. Both the optical gain and the breakdown voltages of SLPT increase with the increasing t_w. The reason is that

the drift-time and the energy of electrons in the well increase with the increasing t_w, this, in turn, leads to an increase of the electron impact ionisation probability and then an increase of optical gain. Also, the optical gain of SLPT increases with the SL period number from 5 to 15, under the same incident light power level and dark current order. This result can be explained by the following argument. With a good interface quality of SL, increasing the period number leads to an increase in multiplication factor, hence an increase of the optical gain. The maximum optical gain obtained is 287 for SLPT with $t_b = 80$ Å, $t_w = 400$ Å and $N = 10$. The peak spectral response of SLPT shifts from 540 to 480 nm when the V_{CE} bias increases from 1 to 4 V. The peak response wavelength for SLPT also shifts to the shorter wavelength when t_w decreases from 500 to 75 Å. There is no sub-peak in the spectral response of SLPT, since SLPT has a higher internal electric field in the collector region which reduces the surface recombination effect at the ITO interface [17].

5 Comparison of phototransistors

Optimum operation of various amorphous phototransistors needs a suitable choice of V_{CE} bias, load resistance, and incident light power level etc. For the purpose of comparison, the optimum performances of the various amorphous phototransistors mentioned are listed in Table 1. The advantages and possible applications for various amorphous phototransistors are also noted in Table 1.

Table 1: Performance comparison of various a-Si:H/a-SiC:H phototransistors

Amorphous phototransistor	Optical gain	Response time (μs)	Features
PT	12	30	Simple structure, first amorphous device having gain
HPT	40	10	colour-sensitivity, comparable in gain to c-Si PT
SHPT	78	4.1	Best photo I-V curves, high BV_{CEO}, linear amplifier
SLPT	287	6.2	Highest and adjustable optical gain

6 APD

Based on the study of the amorphous phototransistors, to improve the performance of the photosensing device with 2 leads further, in analogue to the compound semiconductor devices with SL, it is known that if SL is applied to the avalanche multiplication region of the avalanche photodiode (APD) or reach-through APD (RAPD), the optical gain and noise could be improved. This idea motivated the study of a-Si:H/a-SiC:H SL APD and RAPD. Actually, referring to the energy-band diagram of SHPT, as shown in Fig. 5*b*, if the emitter region of SHPT is replaced by a p^+ amorphous semiconductor layer, a reverse-bias is applied to the resulting device, and the incident light is let onto this p^+ layer, the electron-injection is still obtainable. Then, by employing the multiplication properties of SL, excellent photodiodes could be designed.

An amorphous semiconductor can also be used to fabricate a rectifying diode. Except for the conventional *p-i-n* diode, by using the heterojunction bulk barrier, a unipolar diode (HEBUD) can be fabricated to provide the rectifying function [14]. In HEBUD, a sawtooth-shaped conduction band is obtained by periodically adjusting the composition of intrinsic a-$Si_{1-x}C_x$:H in which the carbon content is graded. The sawtooth-shaped conduction band is an asymmetrical potential barrier and has a property similar to that of the Schottky barrier having a rectifying function. Preliminary results show that the design principle is feasible, the device is fully depleted and stable. A switching time of 15 μs and a propagation delay of 9 μs are obtained. But, under forward bias, the diode ideality factor $n = 2.89$ and 3.12, respectively, for the conduction band having 3 and 5 sawtooth-shaped barriers. These measured *n*s are higher than the values obtained from a good Schottky barrier diode. The HEBUD can be operated at a low voltage or with multiple barriers for high voltage application. The unipolar nature of the device suggests a possible application of this device to high-speed circuits. Moreover, HEBUDs with the capability of barrier-height tailoring should be useful in many applications [21].

7 SAPD

The schematic cross-section and the simplified energy-band diagram under a reverse-bias V_R for electron-injection SAPD are depicted in Figs. 6*a* and *b*, respectively. As shown in Fig. 6*a*, the a-Si:H $t_w = 200$ Å, a-SiC:H $t_b = 280$ Å and the period number $N = 10$ for intrinsic SL. There are three alternative structures for this SAPD. One is that an intrinsic a-Si:H layer may be added between the n^+ a-Si:H (500 Å) and the SL region to increase the device breakdown voltage. The other is that the p^+ a-Si:H (200 Å) may be replaced by a p^+ a-SiC:H layer to enhance the effect of an optical window. Another is that, if p^+ and n^+ a-Si:H layers are interchanged, then the device becomes the complementary hole-injection SAPD. The hole-injection SAPD has poor performance as expected.

Ideally, for a good quality SL structure, the multiplication factor per period (stage) is two. In practice, the multiplication factor per stage is $1 + r$, where r is the ionisation yield (the fraction of carriers ionizing per stage). The total multiplication factor of the SL structure $M = (1 + r)^N$ [23], where N is the period number of SL. To obtain the electron and hole impact-ionization rates, α and β, by the conventional *p-i-n* diode formulas [24], both the electron- and hole-injection SAPDs with a complementary structure are fabricated, and their electron and hole multiplication factors are obtained by the photocurrent multiplication method. The obtained α and β can be approximately expressed by the empirical expressions [22]:

$$\alpha(E) = 8.34 \times 10^4 \, \mathrm{EXP}\,(-2.0998 \times 10^5/E)\,\mathrm{cm}^{-1}$$

$$\beta(E) = 1.789 \times 10^4 \, \mathrm{EXP}\,(-2.7910 \times 10^5/E)\,\mathrm{cm}^{-1}$$

for electric field E in volts per centimetre. When the electric field E is increased from 2.08×10^5 to 2.92×10^5 V/cm, the ratio $K = \alpha/\beta$ decreases from 6.5 to 5.05. This is the first observation of the ionization-rate ratio K in an intrinsic a-Si:H/a-SiC:H SL structure. A higher α and β ratio could be achieved by tailoring the superlattice composition and thickness.

The SAPD has a maximum optical gain of 184. The response time is 4.5 μs. The SAPD is promising in applications of high-sensitivity and high-frequency switching circuits [22].

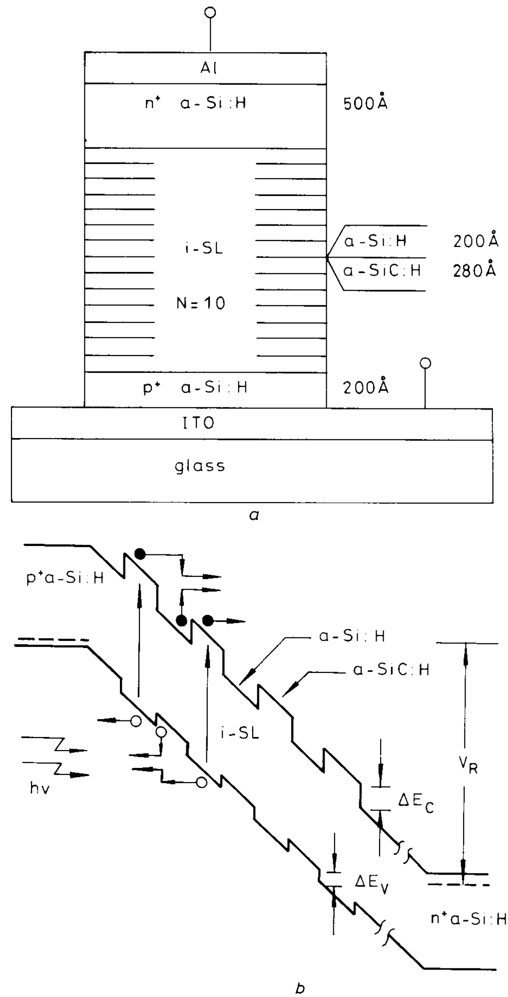

Fig. 6 *Depictions for electron-injection a-Si: H/a-SiC: H SAPD*
a Device cross-section
b Energy-band under reverse-bias V_R

8 SRAPD

Basically, the RAPD has independent light absorption and avalanche regions. This structure has several desirable characteristics not present in the other structures. The tradeoff between the quantum efficiency and response speed can be accurately controlled by adjusting the width of the low-field absorption and drift region. The photocurrent multiplication occurs primarily in the narrow high-field avalanche region. The wide, low-field drift region in the device produces a much more gradual change in the multiplication with the reverse-bias voltage, which is desirable for practical application. So, RAPD has high optical gain, high response speed and a good signal to noise ratio [28]. If the superlattice is applied to the avalanche region, the optoelectronic characteristics could be improved further [18–20].

Figs. 7*a* and *b* illustrate the schematic cross-section and the energy-band diagram under reverse-bias V_R for an electron-injection a-Si:H/a-SiC:H SRAPD, respectively [26]. For the purpose of performance comparison and observation of the SL effects, an electron-injection

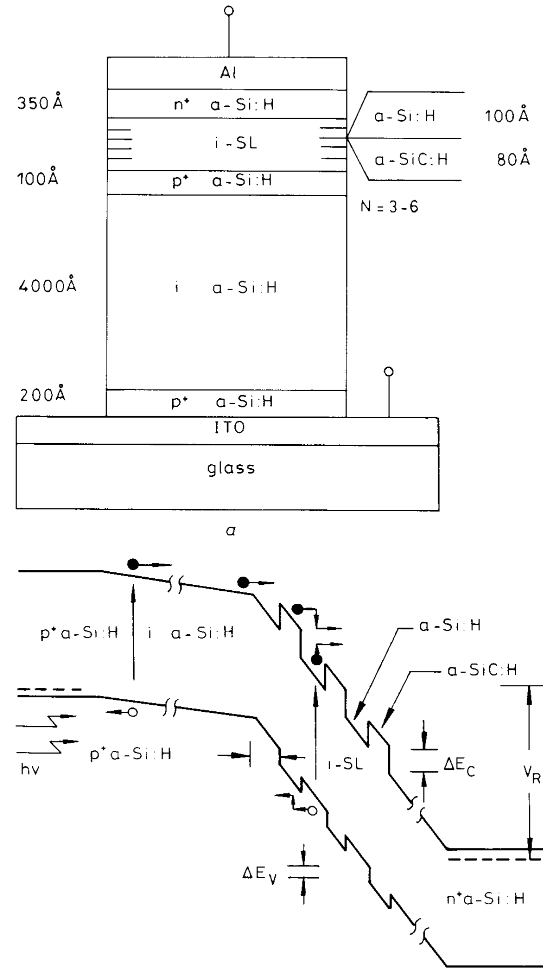

Fig. 7 *Structure and band diagram under V_R for descriptions of electron-injection a-Si: H/a-SiC: H SRAPD*
a Structure
b Band diagram

a-Si:HRAPD with similar device dimensions is also fabricated. In this a-Si:H RAPD the avalanche region is a 400 Å intrinsic a-Si:H layer [27]. The hole-injection a-Si:H/a-SiC:H SRAPD and a-Si:H RAPD are also fabricated to obtain the hole multiplication factors.

Fig. 8 illustrates the electron multiplication factors *M*s, against the applied reverse-bias V_R for the electron-injection a-Si:H/a-SiC:H SRAPD with $N = 3$ and a-Si:H RAPD. It can be seen from the Figure that the electron multiplication factors (>12) increase relatively slowly with increasing reverse-bias above certain voltages (~ 10 V). These voltages could be the reach-through voltages of the devices. The electron multiplication factor of a-Si:H/a-SiC:H SRAPD is generally higher than that of the a-Si:H RAPD [26].

Since the avalanche process predominantly occurs in the high field region, the impact ionization rate α and β for a-Si:H RAPD is estimated from the electron and hole multiplication factors using the well known formulas for *p-i-n* diodes [24]. In a-Si:H/a-SiC:H SRAPD, the ava-

lanche region can be assumed to be only in the a-Si:H well layers, because the ionization threshold energies which are roughly proportional to the band-gap are much higher in a-SiC:H barriers than in a-Si:H wells. Then, the average α and β [29–30] can be shown to be obtainable by these formulas also. The obtained average α and β for a-Si:H/a-SiC:H SRAPD with $N = 3$ can be expressed approximately by the empirical expressions [26]:

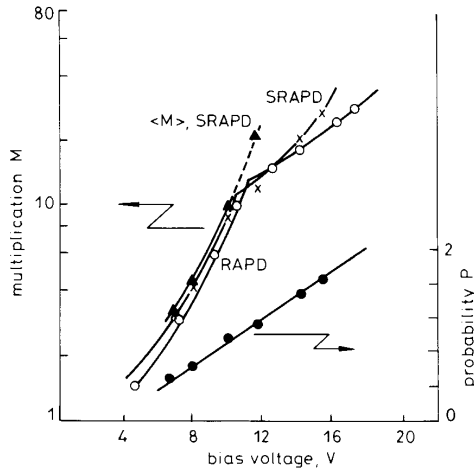

Fig. 8 *Multiplication factors against applied reverse-bias voltage for electron-injection a-Si:H/a-SiC:H SRAPD and a-Si:H RAPD*

The average multiplication $\langle M \rangle$ and electron impact-ionization probability per period, P, for an a-Si:H/a-SiC:H SRAPD are shown also

$$\alpha(E) = 1.14 \times 10^6 \text{ EXP } (-2.05 \times 10^6/E) \text{ cm}^{-1}$$

$$\beta(E) = 1.66 \times 10^5 \text{ EXP } (-3.95 \times 10^6/E) \text{ cm}^{-1}$$

where $E \sim V_R/W$ V/cm, and W is the width of the avalanche region. The impact ionization rate ratio ($K = \alpha/\beta$) is 10.02 at an electric field of 3.33×10^6 V/cm for a-Si:H/a-SiC:H SRAPD, and that for a-Si:H RAPD is 6.95 at the same electric field. This phenomenon demonstrates that the amorphous SL can be used to promote the K value. As compared to the α and β expressions for SAPD, these two equations are applicable in a higher electric-field range. Furthermore, since, in SRAPD, $t_w = 100$ Å and $t_b = 80$ Å which are smaller than those of the SAPD, so the SRAPD has a higher internal field and multiplication factor under the similar reverse-bias level. To verify the obtained ratio $K = \alpha/\beta$, the excess noise factor is calculated for electron-injection a-Si:H/a-SiC:H SRAPD from the noise spectral density measurements. The shot noise is the dominant one. The data of noise spectral densities are taken at a frequency of 40 kHz, which avoids the increase of noise in the lower frequency range [26]. For electron-injection alone, in terms of the well known McIntyre's theory [18], the excess noise factor F can be written as

$$F = K'M + (2 - 1/M)(1 - K')$$

where $K' = 1/K$, so, the ratio K can be obtained from the calculated F and the known M. The obtained K is 11.29 which is approximately the same as the one (10.02) obtained from the photocurrent multiplication method [26].

The excess noise factors calculated by using the above F equation as a function of the multiplication factor at a fixed $K = 10.02$ and 6.95, respectively, for a-Si:H/a-SiC:H SRAPD and a-Si:H RAPD are shown in Fig. 9. The data for a typical c-Si RAPD are also included for comparison [31]. It can be seen from this Figure, that the amorphous SRAPD and RAPD have the higher Fs than that of c-Si RAPD. But, for amorphous devices, SRAPD has a lower F than that of RAPD. The F value of SRAPD is also affected by the width of the high field avalanche region at a fixed operating bias. Experimentally, it is found that the K value increased and F value decreased with the increasing width of the high-field avalanche region [26].

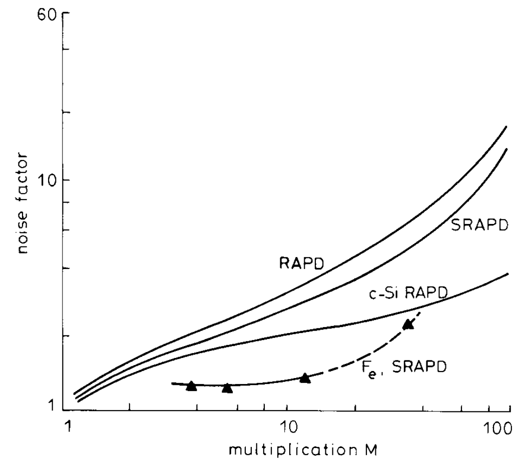

Fig. 9 *Calculated excess noise factors as a function of multiplication factor M for electron-injection a-Si:H/a-SiC:H SRAPD, a-Si:H RAPD and c-Si RAPD*

The estimated F_e for the a-Si:H/a-SiC:H SRAPD is depicted also

The explicit formulas for the excess noise factor F_e and average multiplication $\langle M \rangle$ in double-carrier SAPD with electron injection, assuming the electron impact-ionization probability per period is less than one, are also used to calculate the F_e and $\langle M \rangle$ for a-Si:H/a-SiC:H SRAPD. The electron impact-ionization probability per period $P = \exp(\int_0^L \alpha \, dz) - 1$, where L is the length of each period. Using the average α and β obtained for a-Si:H/a-SiC:H SRAPD, the F_e and $\langle M \rangle$ estimated by using those explicit formulas [32] are shown in Figs. 8 and 9, respectively. For the dashed portions of curves in the Figures, the calculated P is greater than one as shown in Fig. 8. The estimated $\langle M \rangle$ for a-Si:H/a-SiC:H SRAPD is slightly larger than M in the low bias range ($P < 1$) where the $\langle M \rangle$ formula is applicable. The difference between F and F_e for the a-Si:H/a-SiC:H SRAPD is 0.6–2.8. These discrepancies could be due to a-Si:H/a-SiC:H SRAPD having a high electron impact-ionization probability which can lead to improved multiplication and increased excess noise factor [33]. The theory of McIntyre [18] is applied by considering the continuous multiplication region and is shown as F in Fig. 9 [26].

The a-Si:H/a-SiC:H SRAPD exhibited an optical gain of 506 and that for a-Si:H RAPD is 380. The optical gain of the a-Si:H/a-SiC:H SRAPD is the highest one among the amorphous photodetectors ever reported. Both of these devices have a t_{on} time of 1 μs. It is also found that the optical gain increases with the reverse-bias due to the higher impact-ionization rates of the photogenerated carriers. The optical gain and breakdown voltage of the a-Si:H/a-SiC:H SRAPD also increases with the well

thickness when it is varied from 80 to 120 Å. But, the optical gain decreases if the number of SL periods is increased from 3 to 6. Increasing the well thickness would increase the electron energy by increasing its drift length. This, in turn, can increase the impact ionization probability, which increases the optical gain. But, when the well thickness or number of period is increased over a certain limit, the resulting reduction of high electric field in the undoped SL region reduces the obtainable optical gain. The a-Si:H/a-SiC:H SRAPD has high gain, high speed and low noise, so, it is a promising device for photodetector application [26].

9 Comparison of APDs

For the purpose of comparison, the optimum performance of various APDs are given in Table 2. The distinct advantage of each APD is also noted. It can be seen that the amorphous RAPD and SRAPD are the excellent devices for photosensing application.

Table 2: Performance comparison of various a-Si:H/a-SiC:H avalanche photodiodes

Avalanche photodiodes	Optical gain	Response time (μs)	$K = \alpha/\beta$	Features
SAPD	184	4.5	6.5	First reported K in amorphous SL
RAPD	380	1*	6.95	Simple structure, high gain, high speed, tradeoff between quantum efficiency and response speed
SRAPD	560	1*	10.02	High gain, high speed, low noise, comparable in noise to c-Si RAPD

* t_{on} only

10 Conclusion

This paper mainly describes the optoelectronic performances of seven amorphous photosensing devices, i.e. PT, HPT, SHPT, SLPT, SAPD, RAPD, and SRAPD. The PT has the simplest device structure and is the first proposed amorphous device with gain. The HPT possesses the colour-sensitivity and may be used as a voltage-controlled colour-sensitive photodetector. The SHPT has the pretty photo I-V curves and could be used in optoelectronic analogue circuits. The SLPT has the highest optical gain among the various amorphous phototransistors. In the study of SAPD, the electron and hole impact-ionization rates, α and β, are firstly presented for the intrinsic a-Si:H/a-SiC:H SL. The a-Si:HRAPD has a simple structure, and has a higher optical gain and a shorter response time than those of the various amorphous phototransistors. The SRAPD has the advantages of high speed, low noise and the highest optical gain.

The above-mentioned devices can be used in the optocouplers and large-area electronic applications, such as image sensor etc. To match these devices with the specific application, the reliability of these devices, and some of the other amorphous devices, such as LED and TFT, would be studied.

11 Acknowledgments

The authors are grateful to Dr. B.S. Wu, Dr. S.C. Jow, Mr. Y.W. Chen, Mr. K.C. Chang, Mr. M.T. Wu, Mr. W.L. Laih, and Mr. R.H. Lee, for their assistance during research. This work was supported by the National Science Council, Republic of China.

12 References

1 KANICKI, J., ALT, P.M., and HOWARD, W.E.: 'Special issue on amorphous semiconductor devices', *IEEE Trans.*, 1989, **ED-36,** (12)

2 HAMAKAWA, Y.: 'Amorphous semiconductor technologies and devices' (Ohmsha and North-Holland, Amsterdam, 1987)

3 CHANG, C.Y., WU, B.S., FANG, Y.K., and LEE, R.H.: 'Optical and electrical current gain in an amorphous silicon bulk barrier phototransistor', *IEEE Electron Device Lett.*, 1985, **EDL-6,** pp. 149–150

4 WU, B.S., CHANG, C.Y., FANG, Y.K., and LEE, R.H.: 'Amorphous silicon phototransistor on a glass substrate', *IEEE Trans.*, 1985, **ED-32,** pp. 2192–2196

5 WU, B.S., CHANG, C.Y., FANG, Y.K., and LEE, R.H.: 'Amorphous silicon thin film phototransistor'. Proc. 1984 Int. Conf. Solid State Devices Mater., Kobe, Japan, pp. 551–554

6 CHANG, C.Y., WU, B.S., FANG, Y.K., and LEE, R.H.: 'Amorphous silicon bulk barrier phototransistor with Schottky barrier emitter', *Appl. Ohys, Lett.*, 1985, **47,** pp. 49–51

7 CHANG, C.Y., WU, B.S., FANG, Y.K., and LEE, R.H.: 'Amorphous silicon bipolar transistor with high gain (> 12) and high-speed (> 30 μs)'. 1985 Int. Electron Devices Meeting, Washington D.C., U.S.A., pp. 432–435

8 CHANG, C.Y.: 'Photogeneration and recombination in a bulk barrier phototransistor', *IEEE Trans.*, 1986, **ED-33,** pp. 1829–1830

9 MITSUYU, T., FUJITA, S., and SASAKI, A.: 'InGaAsP/InP wavelength-sensitive heterojunction phototransistors', *IEEE Trans.*, 1984, **ED-31,** pp. 812–817

10 CHANG, C.Y., CHANG, K.C., FANG, Y.K., and JOW, S.C.: 'The heterojunction amorphous n^+(a-Si)/n-i-p(a-SiC)/i-n^+(a-Si) phototransistor with high gain (~40) and high speed (~10 μs)'. 1986 Int. Electron Devices Meeting, Los Angeles, U.S.A., pp. 200–204

11 CHANG, C.Y., CHANG, K.C., FANG, Y.K., and JOW, S.C.: 'Amorphous Al/n^+ a-SiC/i a-SiC/p^+ a-SiC/i a-Si/n^+ a-SiC heterojunction phototransistor with high gain and high speed'. Proc. 1986 Int. Conf. Solid State Devices Mater., Tokyo, Japan, pp. 695–698

12 CHANG, K.C., CHANG, C.Y., FANG, Y.K., and JOW, S.C.: 'The amorphous Si/SiC heterojunction color-sensitive phototransistor', *IEEE Electron Device Lett.*, 1987, **EDL-3,** pp. 64–65

13 HONG, J.W., CHEN, Y.W., CHANG, K.C., FANG, Y.K., and CHANG, C.Y.: 'A hydrogenated amorphous Si/SiC heterojunction phototransistor', *Solid-State Electron.*, 1989, **32,** pp. 883–886

14 JOW, S.C., CHANG, C.Y., FANG, Y.K., and WU, M.T.: 'Amorphous Si/SiC superlattice heterojunction phototransistors: a new photodetector suitable for optoelectronic application'. Proc. 1987 Electronic Devices Mater. Symp., Taipei, Taiwan, R.O.C., pp. 215–218

15 WU, M.T., CHANG, C.Y., FANG, Y.K., and LAIH, W.L.: 'Amorphous Si:H/SiC:H superlattice phototransistor'. Proc. 1987 Symp. Solar Energy Society, R.O.C., pp. 77–88

16 CHANG, C.Y., FANG, Y.K., HONG, J.W., JOW, S.C., and LAIH, W.L.: 'Amorphous Si/SiC phototransistors'. Proc. 1987 Workshop on Semiconductor Defect Physics and Engineering, Tainan, Taiwan, R.O.C., pp. 151–167

17 WU, M.T., FANG, Y.K., HONG, J.W., and CHANG, C.Y.: 'Hydrogenated amorphous Si/SiC superlattice phototransistors'. to be published in *Solid-State Electron*

18 McINTYRE, R.J.: 'Multiplication noise in uniform avalanche diodes', *IEEE Trans.*, 1966, **ED-13,** pp. 164–168

19 MATSUO, K., TEICH, M., and SALCH, B.E.A.: 'Noise and time response of the staircase avalanche photodiode', *IEEE Trans.*, 1985, **ED-32,** pp. 2615–2623

20 BRENNAN, K., WANG, T., and HESS, K.: 'Theory of electron impact ionization including a potential step: Application to GaAs-AlGaAs', *IEEE Electron Device Lett.*, 1985, **EDL-6,** pp. 199–201

21 JOW, S.C., and CHANG, C.Y.: 'Amorphous silicon/silicon carbide heterojunction bulk unipolar diodes (HEBUD)', *IEEE Electron Device Lett.*, 1986, **EDL-7,** pp. 689–691

22 JOW, S.C., WU, M.T., FANG, Y.K., CHEN, Y.W., HONG, J.W., and CHANG, C.Y.: 'Amorphous silicon/silicon carbide superlattice avalanche photodiodes', *IEEE Trans.*, 1988, **ED-35**, pp. 1279–1283
23 CAPASSO, F., TSANG, W.T., and WILLIAMS, G.F.: 'Staircase solid-state photomultipliers and avalanche photodiodes with enhanced ionization rate ratio', *IEEE Trans.*, 1983, **ED-30**, pp. 381–390
24 STILLMAN, G.E., and WOLFE, C.M.: 'Avalanche photodiodes', *in* WILLARDSON, R.K., and BEER, A.C. (Eds.): 'Semiconductors and semimetals' (Academic, New York, 1977), p. 333
25 LAIH, W.L., CHEN, Y.W., JOW, S.C., FANG, Y.K., and CHANG, C.Y.: 'A high-gain low-noise amorphous Si/SiC superlattice reach-thorough avalanche photodiode'. Proc. 1988 Int. Electronic Devices Mater. Symp., Kaohsiung, Taiwan, R.O.C., pp. 12–15
26 HONG, J.W., LAIH, W.L., CHEN, Y.W., FANG, Y.K., CHANG, C.Y., and GONG, J.: 'Optical and noise characteristics of amorphous Si/SiC superlattice reach-through avalanche photodiodes', *IEEE Trans.*, 1990, **ED-37**, pp. 1804–1808
27 HONG, J.W., CHEN, Y.W., LAIH, W.L., FANG, Y.K., CHANG, C.Y., and GONG, J.: 'The hydrogenated amorphous silicon reach-through avalanche photodiodes (a-Si:H RAPD's)', *IEEE J. Quantum Electronics*, 1990, **26**, pp. 280–284
28 SZE, S.M.: 'Physics of semiconductor devices' (Wiley, New York, 1981), 2nd edn., Chap. 13
29 CAPASSO, F., TSANG, W.T., HUTCHINSON, A.L., and WILLIAMS, G.F.: 'Enhancement of electron impact ionization in superlattice: A new avalanche photodiode with large ionization rate ratio', *Appl. Phys. Lett.*, **40**, 1982, pp. 38–40
30 OSAKA, F., MIKAWA, T., and WADA, O.: 'Electron and hole impact ionization rates in $InP/Ga_{0.47}IN_{0.53}As$ superlattice', *IEEE J. Quantum Electron.*, 1986, **QE-22**, pp. 1986–1991
31 GOWAR, J.: 'Optical fibre communication' (Prentice-Hall, London, 1984), Chap. 13
32 TEICH., M.C., MATSUO, K., and SALEH, B.E.A.: 'Excess noise factors for conventional and superlattice avalanche photodiodes and photomultiplier tubes', *IEEE J. Quantum Electron.*, 1986, **QE-22**, pp. 1184–1193
33 FYATH, R.S., and O'REILLY, J.J.: 'Effect on the performance of staircase APD's of electron impact ionization within the graded-gap region', *IEEE Trans.*, 1988, **ED-35**, pp. 1357–1363